

# Efficient formation of strongly bound ultracold cesium molecules by photoassociation with tunneling

Mihaela Vatasescu<sup>1</sup>, Claude M Dion<sup>2</sup> and Olivier Dulieu<sup>3</sup>

<sup>1</sup> Institute of Space Sciences, MG-23, RO-77125, Magurele-Bucharest, Romania

<sup>2</sup> Department of Physics, Umeå University, SE-901 87 Umeå, Sweden

<sup>3</sup> Laboratoire Aimé Cotton, CNRS, Bâtiment 505, Univ. Paris-Sud, 91405 Orsay-Cedex, France

E-mail: olivier.dulieu@lac.u-psud.fr

**Abstract.** We calculate the rates of formation and detection of ultracold Cs<sub>2</sub> molecules obtained from the photoassociation of ultracold atoms through the double-well  $0_g^-(6S_{1/2} + 6P_{3/2})$  state. We concentrate on two features previously observed experimentally and attributed to tunneling between the two wells [Vatasescu et al 2000 Phys. Rev. A **61** 044701]. We show that the molecules obtained are in strongly bound levels ( $v'' = 5, 6$ ) of the metastable  $a^3\Sigma_u^+(6S_{1/2} + 6S_{1/2})$  ground electronic state.

Submitted to: *J. Phys. B: At. Mol. Phys.*

## 1. Introduction

The control of elementary interactions between atoms or molecules in the gas phase is a long term concern for researchers, namely in order to find ways towards the full control of a chemical reaction, giving the ability to choose the reaction path unambiguously from a well-defined internal state towards a desired final state. In this context, laser cooling and trapping of atoms has opened an entirely new field of investigation, as they can be brought almost to rest, in a well-defined internal state. A spectacular example is provided by the observation of Bose-Einstein condensation in alkali gases [1, 2, 3], recently followed by the demonstration of quantum degeneracy in a fermionic alkali gas [4].

Slowing and cooling of molecules, despite the inherent difficulty caused by the complex internal molecular structure, represents an increasingly active research field with many achievements since the first observation of ultracold  $\text{Cs}_2$  molecules by photoassociation of laser-cooled cesium atoms [5]. Two approaches have been proven to be very efficient, namely Stark deceleration [6] and buffer gas cooling [7]. Other promising methods rely on phase space filtering of a molecular beam [8], on billiard-like collisions [9], or on a gas expansion out of a rotating nozzle [10]. A major breakthrough has been the observation of molecular Bose-Einstein condensates, using magnetic field tunability of Feshbach resonances [11, 12]. Also, two groups recently measured for the first time rates for collisions between ultracold cesium atoms and cesium molecules [13, 14].

Among the various approaches, the photoassociation (PA) process is very attractive, as it starts from a pair of ultracold atoms which absorbs a photon to form an ultracold molecule in a short-lived excited electronic state [15]. The main drawback is that the stabilization of the excited molecule into stable electronic states hardly provides an ensemble of molecules in a well-defined internal state, as it relies on spontaneous emission which populates many vibrational levels. Some attempts to use stimulated emission have been reported [16, 17], but they were limited to the transition into high-lying levels. Indeed, due to the poor spatial overlap of the wave function of the photoassociated level — predominant at large interatomic distances — with the wave function of the lowest vibrational levels of the stabilized molecules, it is very difficult to create a significant proportion of ultracold molecules in their absolute ground state. A first indication of the possibility to form ultracold molecules in their absolute ground state has been provided in [18] for  $\text{K}_2$  molecules using a two-step photoassociation process. Very recently, a multistep excitation/deexcitation scheme has been set up to produce a fair amount of  $\text{RbCs}$  ultracold molecules in the  $v = 0$  level of the electronic ground state [19].

The purpose of this paper is to describe a possible way to fill these objectives, in the particular case of the formation of ultracold  $\text{Cs}_2$  molecules, using a single-step excitation scheme. It results from the cooperative action of photoassociation at large distances, tunneling and resonant spin-orbit coupling at short distances, and final stabilization by spontaneous decay towards a few low-lying vibrational levels of a stable

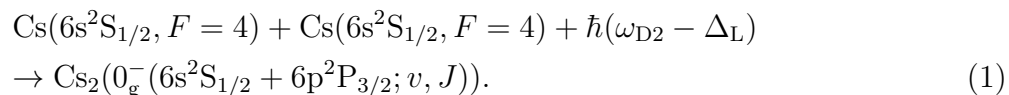
molecular state. We first invoked such a process for the interpretation of so-called ‘‘giant lines’’ observed in photoassociation spectra in [20], hereafter referred to as paper I. One of us also performed a time-dependent analysis of the tunneling process in such ultracold conditions, helpful for the determination of the characteristic times of the tunneling motion [21]. From the present calculations involving the available extensive photoassociative spectroscopy of  $\text{Cs}_2$ , we demonstrate that the ultracold molecules are created with a very narrow distribution of vibrational levels, peaking at  $v'' = 5, 6$  of the theoretical potential curve of the  $\text{Cs}_2$  metastable triplet state. This could be the first example of the formation of ultracold molecules left mainly in a single deep vibrational level via single-photon PA. The possibility to use this mechanism to create the initial state of cesium dimers in ultracold collisions with cesium atoms has been discussed in ref.[13].

We present our calculation of the photoassociation rate, of the cold molecule formation rate, and of the molecular ion signal resulting from the photoionization of the stabilized cold molecules. This emphasizes the role of the detection process in the interpretation of the strong intensity of these giant lines observed in the photoassociation spectrum.

We start in section 2 by recalling the main facts concerning the tunneling effects in the photoassociation of  $\text{Cs}_2$ . We then present the model used to calculate the molecule formation rates (section 3), followed by the results of the simulations for the  $\text{Cs}_2^+$  ionization signals (section 4). Finally, concluding remarks are given in section 5.

## 2. Experimental and theoretical facts on giant lines and tunneling in the PA of cesium

We briefly recall below the main results of paper I. The PA process between two ultracold cesium atoms in a magneto-optical trap (MOT), shown in figure 1, is written as



The pair of cold cesium atoms absorbs a photon detuned by  $\Delta_L$  to the red of the D2 atomic transition frequency  $\omega_{D2}$ , to populate rovibrational levels of the external well of the double-well-shaped  $0_g^-$  molecular state correlated to the  $6S_{1/2} + 6P_{3/2}$  dissociation limit (hereafter labeled  $0_g^-(P_{3/2})$ ). These levels are detected by two well-established methods: first through the fluorescence variations of the atomic trap induced by their spontaneous decay towards bound levels or towards the dissociation continuum of the lowest  $a^3\Sigma_u^+(6S_{1/2} + 6S_{1/2})$  state, second through the resonant two-photon ionization (R2PI) of the ultracold molecules formed in this metastable triplet state into  $\text{Cs}_2^+$  molecular ions. The latter method delivers a very neat spectrum with excellent signal-to-noise ratio. Typical experimental conditions are temperatures between 20 and 200  $\mu\text{K}$ , a mean atomic density of about  $4 \times 10^{10} \text{ cm}^{-3}$  with a peak density of  $10^{11} \text{ cm}^{-3}$ , the number of atoms being estimated between 2 to  $5 \times 10^7$  atoms, and intensities of 50

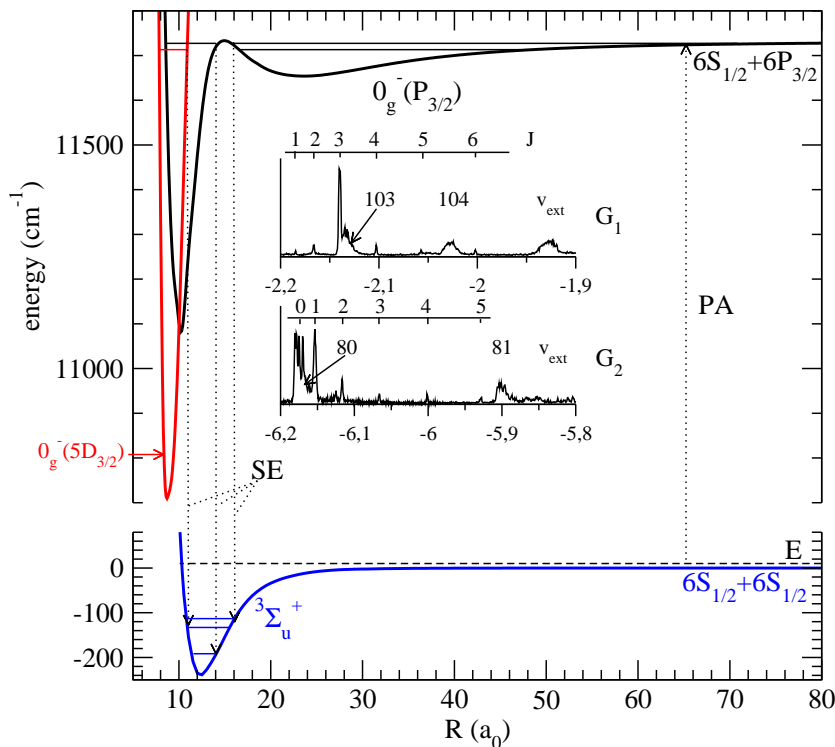


**Figure 1.** Scheme of the photoassociation (PA) process and subsequent spontaneous emission (SE) of the  $0_g^-(P_{3/2})$  excited molecule to the metastable  $a^3\Sigma_u^+(6S_{1/2} + 6S_{1/2})$  state. The  $0_g^-(P_{3/2})$  state is coupled to the  $0_g^-(5D_{3/2})$  via spin-orbit interaction. Vibrational levels involved in the tunneling through the  $0_g^-(P_{3/2})$  barrier, as well as the deep  $a^3\Sigma_u^+$  vibrational levels which can be reached by spontaneous decay are pictured with lines (not to scale). The recorded experimental spectrum is recalled in the two insets, for both the  $G_1$  and  $G_2$  features, showing their large rotational structure, and the neighboring levels  $v_{\text{ext}}$  of the  $0_g^-(P_{3/2})$  external well.

up to  $500 \text{ W/cm}^2$  for the the photoassociation laser [22]. The full R2PI spectrum for the  $0_g^-(P_{3/2})$  has been analyzed in [23], yielding a very precise determination of the corresponding potential curve through the Rydberg-Klein-Rees (RKR) analysis, and through an approach based on the asymptotic modeling of the atom-atom interactions [24]. Vibrational levels from  $v_{\text{ext}} = 0$  to  $v_{\text{ext}} = 132$  have been identified [25] in the  $0_g^-(P_{3/2})$  outer well, with a rotational structure (up to  $J = 4$ ) clearly visible up to  $v_{\text{ext}} = 72$ .

In addition, two intense structures with a large rotational splitting (hereafter referred to as “giant lines”, following paper I, and labeled  $G_1$  and  $G_2$ ) are superimposed on lines associated with levels of the  $0_g^-$  external well (figure 1). The most intense line within the  $G_1$  ( $G_2$ ) feature was assigned to  $J = 3$  ( $J = 0, 1$ ) at  $\Delta_L = -2.14 \text{ cm}^{-1}$  ( $\Delta_L = -6.15 \text{ cm}^{-1}$ ) superimposed on  $v_{\text{ext}} = 103$  ( $v_{\text{ext}} = 80$ ), while weak lines assigned up to  $J = 6$  were detected providing a rotational constant  $B_v^{G_1} = 137 \pm 4 \text{ MHz}$  ( $B_v^{G_2} = 243 \pm 8 \text{ MHz}$ ).

With the help of a coupled-channel model, the  $G_1$  and  $G_2$  features have been

assigned in paper I to levels which tunnel through the potential barrier between the two wells of the  $0_g^-(P_{3/2})$  state, as schematized in figure 1. Their large rotational structure is induced by the vibrational motion in two coupled vibrational levels of the  $0_g^-(P_{3/2})$  internal well, which is coupled to several levels in the external well (only two of them are drawn in figure 1 for better clarity). The tunneling effect, unusual for a heavy molecule like  $\text{Cs}_2$ , is then an efficient mechanism to transfer the vibrational motion of the photoassociated state from large interatomic distances towards the inner zone: in contrast with the long-range molecular states usually reached by PA, spontaneous emission of the tunneling levels can stabilize the photoassociated molecules into low vibrational levels of the  $a^3\Sigma_u^+$  metastable state, creating then ultracold molecules with a rather cold vibrational motion. Let us note that the internal state of the molecules created has not been probed experimentally yet.

The  $0_g^-(P_{3/2})$  outer well is represented by the asymptotic model of [24]. As there is no available spectroscopic determination of the  $0_g^-(P_{3/2})$  inner well, this external well is matched to the curve computed by Spies and Meyer [26], through a potential barrier whose height and position have been adjusted in paper I in order to reproduce the experimental observations. The potential barrier then culminates at  $2 \text{ cm}^{-1}$  above the  $6S_{1/2} + 6P_{3/2}$  dissociation limit. Furthermore, according to [26], the  $0_g^-(P_{3/2})$  state is coupled in the inner well region to the next  $0_g^-(6S_{1/2} + 5D_{3/2})$  state (hereafter labeled  $0_g^-(5D_{3/2})$ ) through a non-adiabatic coupling generated by spin-orbit interaction. The  $0_g^-(P_{3/2})$  and  $0_g^-(5D_{3/2})$  curves then exhibit a well-localized avoided crossing around  $10a_0$ , which we transformed into a real crossing by linearizing the curves around the crossing to determine the corresponding standard Landau-Zener coupling parameters. We imposed a finite range for the coupling using the Gaussian form  $A \exp[-(r - r_0)^2/w^2]$  with  $r_0 = 10.02$ ,  $w = 2$ , and  $A = 0.000258$  (all in atomic units). We recall that the absence of resonant coupling between levels of the internal wells would result to a single tunneling level, instead of the two levels assigned in the experiment [20].

For each value of  $J$ , the radial Schrödinger equation is solved with the Mapped Fourier Grid Hamiltonian (MFGH) method [27], providing accurate vibrational energies  $E_{v,J}$ , wave functions  $\chi_{v,J}(R)$ , and rotational constants  $B_{v,J} = \langle \chi_{v,J} | \hbar^2 / (2\mu R^2) | \chi_{v,J} \rangle$  (where  $\mu = 121135.83$  a.u. is the  $\text{Cs}_2$  reduced mass) of the two coupled state. It is well known that tunneling through a potential barrier is very sensitive to its shape and to the position in energy with respect to the top of the barrier. These effects are magnified here as the two tunneling levels of the  $0_g^-(P_{3/2})$  and  $0_g^-(5D_{3/2})$  internal wells, hereafter referred to as  $v_{6P}$  and  $v_{5D}$ , respectively, interact resonantly with the dense — but not continuous — energy level spectrum of the external well. Our calculations predict that the tunneling effect will be observable in the detection signal if the tunneling probability is maximum, which is achieved by adjusting the relative position of the two internal wells to create an almost half-and-half mixing of the  $v_{6P}$  and  $v_{5D}$  radial wave functions. Our model actually presents many tunable parameters for such an adjustment: indeed, the internal well of the potentials, as well as their coupling, are unknown experimentally,

so that their fine tuning is quite tedious. We also noted that the tunneling effect is very sensitive to the value of  $J$ . In order to facilitate the convergence, we stopped the adjustment when we found maximal tunneling for an arbitrary  $J$  value. In other words, we also considered the rotational number  $J$  as a tunable parameter, which we will label as  $\bar{J}$  in the following. An example of the resulting wave functions is shown in figure 2), where the maximal tunneling effect is found for the value  $\bar{J} = 5$ . This is clearly not in agreement with the rotational quantum number of the experiment, but we only need *radial* wave functions for the rate calculations of the next section, which will be evaluated without any  $J$  dependence. The corresponding numerical data is available on request from the authors.

Even if in the adjustment procedure above we used  $\bar{J}$  as a parameter, figure 3 shows that the selectivity of the tunneling process is very strongly dependent on the rotational level. The value of  $B_{v,J}$  defined above is very sensitive to the repartition of the wave function inside the two wells, and panel (a) in figure 3 reflects the pattern shown in figure 2, where the value for  $\bar{J} = 5$  is intermediate between the rotational constant of levels in the internal well ( $\approx 0.008 \text{ cm}^{-1}$ ) and of levels of the external well ( $\approx 0.0005 \text{ cm}^{-1}$ ). Similarly, the  $\bar{J} = 3$  line for  $G_1$  also reflects the extension of the wave function over both wells. The  $\bar{J} = 5$  line displays the same behavior, which can be understood since the rotational structure of  $G_1$  has the same magnitude as the energy spacing between vibrational levels of the external well, so that it is resonant with  $v_{\text{ext}} = 104$  in our calculations. This aspect was not present in the model we set up in paper I and confirms what is observed experimentally. Indeed, due to the ultracold temperature, the s-wave regime is expected to dominate the initial collision between the two Cs atoms (yielding  $J = 0, 1, 2$ ) with probably a small contribution of the p wave (yielding  $J = 1, 2, 3$ ). The presence of higher values of  $J$  at such low temperatures is not yet fully understood [25]. The relative intensities of the  $J = 0, 1, 2$  experimental lines approximately reflects their  $2J + 1$  degeneracy, and the  $J = 2$  line has indeed the strongest intensity for most of the PA lines assigned to the levels of the  $0_g^-(P_{3/2})$  external well. The lines with larger  $J$  values are weaker, due to the small contribution of higher partial waves involved in the collision. We see that this hierarchy is not preserved for  $G_1$  and  $G_2$ : the intense lines are associated with those rotational levels which are indeed resonant with a level of the internal well, i.e.,  $J = 3$  and  $J = 0, 1$ , respectively.

### 3. Photoassociation and cold molecule formation rates for tunneling levels

The metastable  $a^3\Sigma_u^+(6S_{1/2} + 6S_{1/2})$  state is represented by the potential curve of [28], matched beyond  $20a_0$  to the standard asymptotic expansion  $\sum C_n/R^n$  ( $n = 6, 8, 10$ ), with  $C_n$  coefficients taken from [29]. The repulsive wall of the potential is slightly changed in order to reproduce a large and positive scattering length [30]. We work here with  $a_T = 2370a_0$ , which satisfactorily reproduces the intensity envelope of the PA spectrum of [25]. The initial scattering radial wave function is computed through a standard Numerov integration at an energy  $E/k_B T = 150 \text{ } \mu\text{K}$  above the  $6S_{1/2} + 6S_{1/2}$

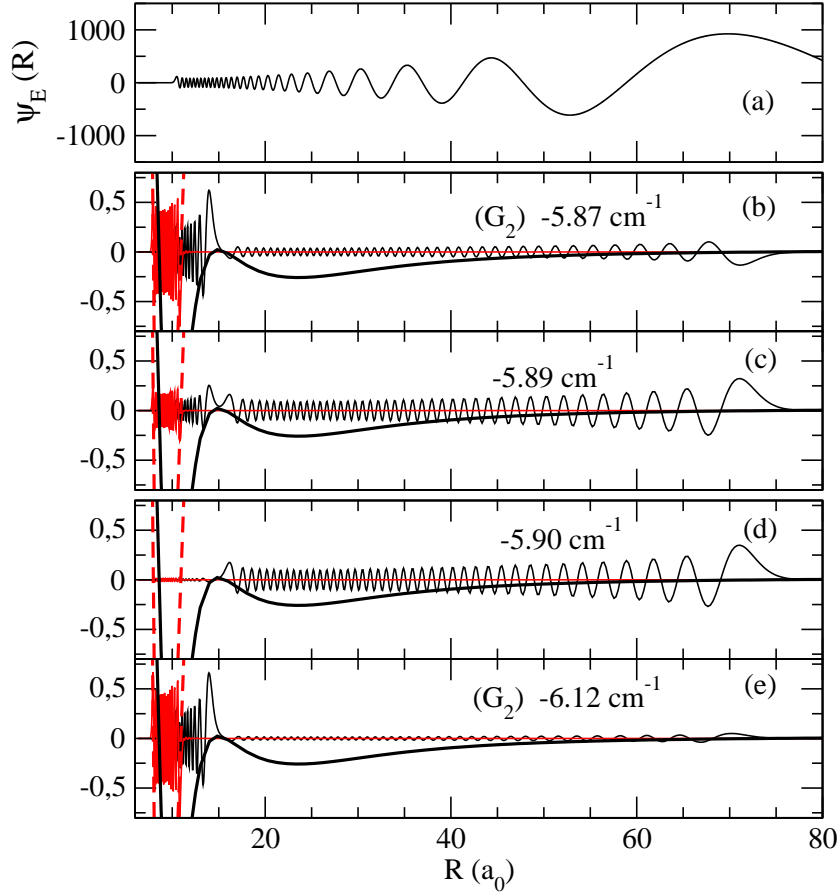


**Figure 2.** Two-channel vibrational wave functions  $\chi_{\bar{v}, \bar{J}}(R)$  (panels b-e) associated with the radial motion in the  $0_g^-(P_{3/2})$  double well (in black) and in the  $0_g^-(5D_{3/2})$  well (in red). The corresponding potentials are drawn with full black and dashed red lines, respectively, to make more visible the extension of the wave functions within the corresponding potentials. The  $\bar{J} = 5$  value (panels b and c) allows maximal tunneling for the  $G_2$  resonance at  $-5.87 \text{ cm}^{-1}$ , almost degenerate with a level of the external well at  $-5.89 \text{ cm}^{-1}$ : the wave functions have significant amplitude over the barrier range. The  $\bar{J} = 0$  case (panels d and e) is also shown for comparison: the energy matching is less favorable and the wave functions hardly penetrate the potential barrier. Panel (a) displays a typical radial wave function of the initial collisional state for a temperature of  $150 \mu\text{K}$ , in the  $a^3\Sigma_u^+(6S_{1/2} + 6S_{1/2})$  state, designed here with a scattering length of about  $2370a_0$ .

asymptote, ignoring the hyperfine structure (figure 2a). Let us note that the accuracy of the  $a_T$  and  $C_n$  values is not crucial for the following calculation of the rates, which can be determined experimentally typically within a factor of 2.

The photoassociation and cold molecule formation rates are evaluated according to the perturbative model already presented in previous papers [22, 31, 32]. Briefly, the photoassociation rate  $R_{\text{PA}}(\bar{v}, \bar{J}; T)$  per atom (expressed in  $\text{s}^{-1}$ ) for an initial continuum state with energy  $E = k_B T$  and wave function  $\psi_E(R)$  into a vibrational level  $\bar{v}$  with a radial wave function  $\chi_{\bar{v}, \bar{J}}(0_g^-; R)$  of the coupled  $0_g^-$  states (where  $\bar{v}$  stands for the quantum number  $v$  of the  $0_g^-(P_{3/2})$  external well levels, or for  $G_1$  or  $G_2$ ), at a detuning

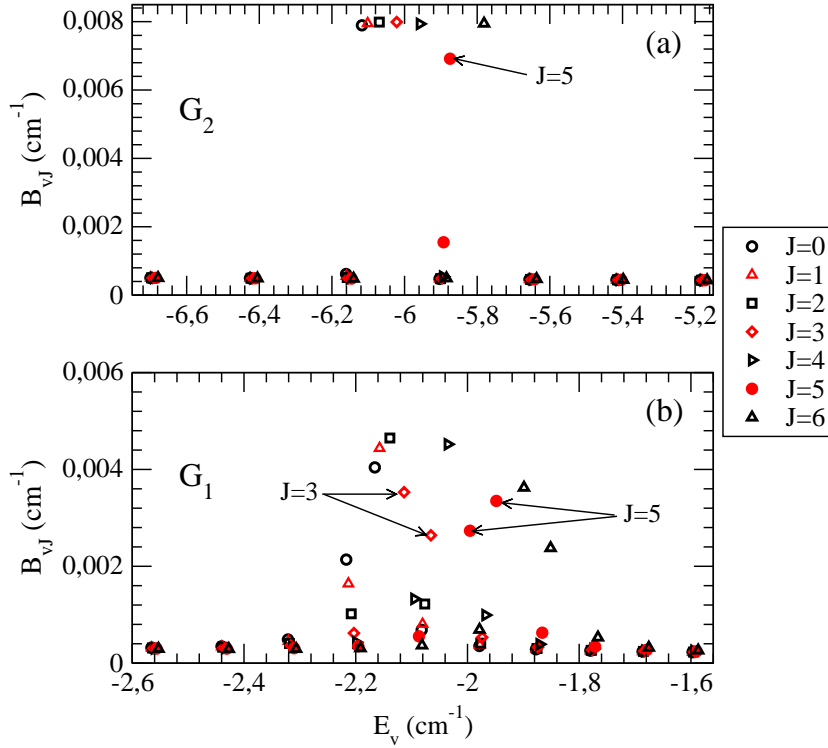


**Figure 3.** Rotational constants  $B_{vJ} = \langle \chi_{\bar{v},\bar{J}} | \hbar^2(2\mu R^2) | \chi_{\bar{v},\bar{J}} \rangle$  for rovibrational levels of the coupled  $0_g^-(6S_{1/2} + 6P_{3/2})$  and  $0_g^-(6S_{1/2} + 5D_{3/2})$  potentials, as function of their binding energy. (a)  $G_2$  structure; (b)  $G_1$  structure. The levels with an important tunneling effect are marked by arrows.

$\Delta_v$  below  $6S_{1/2} + 6P_{3/2}$  limit is expressed as

$$R_{\text{PA}}(\bar{v}, \bar{J}; T) = \left( \frac{3}{2\pi} \right)^{3/2} \frac{\hbar}{2} n_{\text{at}} \lambda_{\text{th}}^3 e^{-\frac{E}{k_B T}} \mathcal{A} K^2 \left| \langle \psi_E | \chi_{\bar{v},\bar{J}}(0_g^-) \rangle \right|^2, \quad (2)$$

where  $n_{\text{at}}$  is the atomic density and  $\lambda_{\text{th}} = \hbar \sqrt{1/(3\mu k_B T)}$  is the thermal de Broglie wavelength. The atomic Rabi frequency  $2K$  is related to the intensity  $I$  of the laser through  $K^2 = \frac{\Gamma}{8} \frac{I}{I_0}$ , where  $\Gamma/2\pi = 5.22$  MHz is the natural width of the  $6P_{3/2}$  atomic level. At the PA wavelength considered,  $\lambda_{\text{PA}}$ , the saturation intensity  $I_0 = \pi \hbar c \Gamma / (3\lambda_{\text{PA}}^3)$  is  $1.1$  mW/cm<sup>2</sup>. The angular factor  $\mathcal{A} = 125/3888$  includes hyperfine degeneracies, assuming an initial  $(F = 4) + (F = 4)$  hyperfine state. As mentioned above, we actually solve the Schrödinger equation for every chosen value of the rotational quantum number  $\bar{J}$  taken as an effective parameter, so we don't include the degeneracy factor  $2J + 1$  in the rate formulas.

The two components of the PA level wave function  $|\chi_{\bar{v},\bar{J}}(0_g^-; R)\rangle$  (see figure 2) are denoted by  $\chi_{\bar{v},\bar{J}}^{6P}(R)$  and  $\chi_{\bar{v},\bar{J}}^{5D}(R)$ , such that

$$O(E, \bar{v}, \bar{J}) \equiv \left| \langle \psi_E | \chi_{\bar{v},\bar{J}}(0_g^-) \rangle \right|^2 = \left| \langle \psi_E | \chi_{\bar{v},\bar{J}}^{6P} \rangle + \langle \psi_E | \chi_{\bar{v},\bar{J}}^{5D} \rangle \right|^2. \quad (3)$$

Following [33], the rate  $R_{\text{mol}}(\Delta_L)$  for cold molecule formation after PA in the  $\bar{v}$  level is obtained by multiplying the PA rate with the branching ratio  $R_{\text{br}}(\bar{v}, \bar{J})$  of the  $\bar{v}$  level



towards the bound levels  $v''(\text{a}^3\Sigma_{\text{u}}^+)$  of the metastable triplet state, and neglecting here the  $R$  dependence of the dipole transition function for the spontaneous decay step,

$$R_{\text{mol}}(\Delta_{\text{L}}) = R_{\text{PA}}(\Delta_{\text{L}})R_{\text{br}}(\bar{v}, \bar{J}), \quad (4)$$

with

$$R_{\text{br}}(\bar{v}, \bar{J}) = \sum_{v''} \left| \langle \chi_{\bar{v}, \bar{J}}(0_{\text{g}}^-) | \phi_{v''}(\text{a}^3\Sigma_{\text{u}}^+) \rangle \right|^2. \quad (5)$$

Figure 4a displays the overlap between the continuum wave function and the bound states of coupled potentials, equation (3), lying in the energy interval between  $-9$  and  $-1.5 \text{ cm}^{-1}$ , for both  $J = 0$  and  $J = 5$ . As expected,  $G_1$  and  $G_2$  have smaller overlap with the initial continuum than the external well levels, due to the weaker probability of wave functions to be localized at large distances. In contrast with the PA rate, the branching ratio of the  $G_1$  and  $G_2$  wave functions is enhanced due to their good localization at short distances (figure 4b). As it was often emphasized, a good production of cold molecules requires a favorable ratio between free-bound and bound-bound transitions. The product  $O(E, \bar{v}, \bar{J}) \times R_{\text{br}}(\bar{v}, \bar{J})$  is represented in figure 4c. If for  $G_1$  the efficiency seems certain, we see that for  $G_2$  this balance is fragile and depends indeed on the  $\bar{J}$  value which makes tunneling effective. On the right axis of this figure is reported the rate for cold molecule formation, equation (4), for typical experimental conditions  $n_{\text{at}} = 10^{11} \text{ cm}^{-3}$  and a PA laser intensity  $I = 100 \text{ W/cm}^2$ . It is found two times and eight times larger than the rate for the  $v_{\text{ext}}$  levels for  $G_2$  and  $G_1$ , respectively. Even if in the experiment the intensities of the  $G_2$  and  $G_1$  lines are found to be comparable (see insets in figure 1), our results confirm that the cold molecule formation rate is indeed larger than the rate for the  $v_{\text{ext}}$  levels. The relative intensity of the  $G_2$  and  $G_1$  lines may be influenced by the two-photon ionization used for the detection (see next section). Let us note also that the rate computed for the  $v_{\text{ext}}$  levels is in agreement with the one reported in [22], where  $R_{\text{mol}} \approx 0.2 \text{ s}^{-1}$  was measured at a detuning of  $7 \text{ cm}^{-1}$ , for a PA laser intensity  $I = 55 \text{ W/cm}^2$ .

The rates for formation of cold molecules in individual levels  $v''$  of the metastable  $\text{a}^3\Sigma_{\text{u}}^+$  state,

$$R_{\text{mol}}(\Delta_{\text{L}}, v'') = R_{\text{PA}}(\Delta_{\text{L}}) \left| \langle \chi_{\bar{v}, \bar{J}}(0_{\text{g}}^-) | \phi_{v''}(\text{a}^3\Sigma_{\text{u}}^+) \rangle \right|^2, \quad (6)$$

are represented in figure 5 for the same range of detunings and same experimental conditions as in figure 4c, for both the  $G_1$  and  $G_2$  features, considering the levels indicated by arrows in figure 4b corresponding to  $\bar{J} = 5$ . Both vibrational distributions peak markedly at  $v'' = 5, 6$ , confirming the efficiency of the PA into the tunneling resonances to produce cold molecules in very low vibrational levels.

#### 4. Modeling the ionization signal

In cesium PA experiments [5, 20], the cold molecules are detected via a two-photon ionization process, where the first photon is resonant with rovibrational levels of

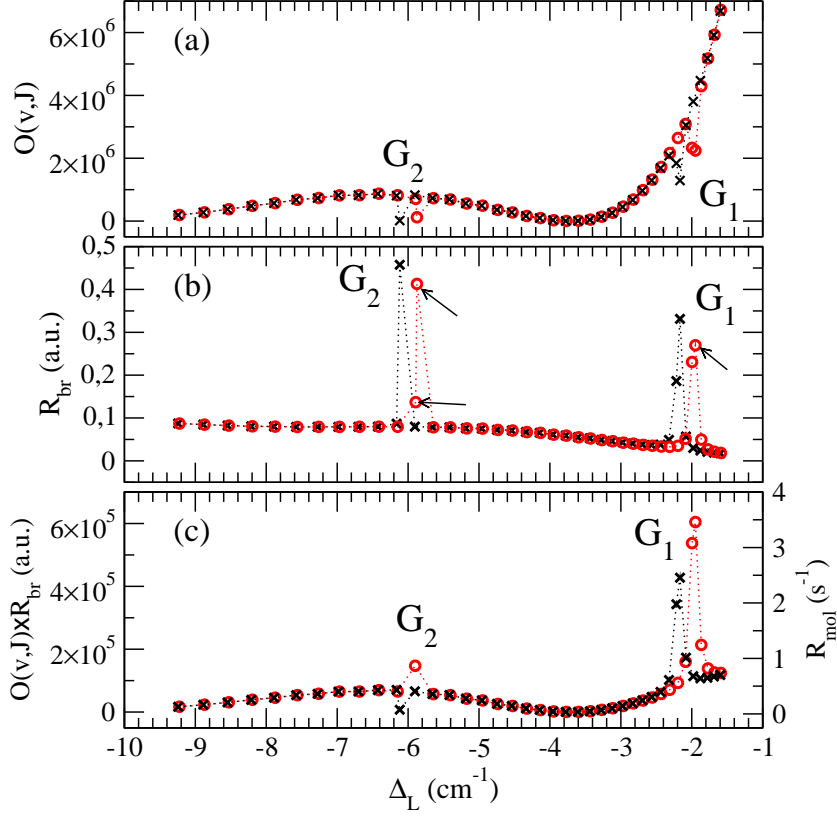


**Figure 4.** (a) Overlap  $O(E, \bar{v}, \bar{J})$  between the continuum wave function and vibrational wave functions of coupled  $0_g^-$  potentials lying in the detuning interval between  $-9$  and  $-1.5$   $\text{cm}^{-1}$ . (b) Branching ratio  $R_{\text{br}}(\bar{v}, \bar{J})$  of the same levels to the  $a^3\Sigma_u^+$  vibrational states. (c) Product of the two previous quantities (left axis) and corresponding cold molecule formation rate  $R_{\text{mol}}(\Delta_L)$  (right axis) assuming an atomic density  $n_{\text{at}} = 10^{11}$   $\text{cm}^{-3}$  and a PA laser intensity  $I = 100$   $\text{W}/\text{cm}^2$ . Note that in this panel the contribution of the nearby levels at  $-5.87$   $\text{cm}^{-1}$  and  $-5.89$   $\text{cm}^{-1}$  shown in figure 2 are added together into a single rate value around  $-5.9$   $\text{cm}^{-1}$ . Both  $\bar{J} = 0$  (black crosses) and  $\bar{J} = 5$  (red open circles) are shown. The levels corresponding to  $G_1$  and  $G_2$  are indicated. The arrows identify the levels for which we calculated the vibrational distribution of the produced cold molecules displayed in the figure 5.

molecular states correlated to the  $6S_{1/2} + 5D_{3/2}$  dissociation limit. Therefore, the ionization signal is very sensitive to the wavelength chosen for the ionization laser. Following our previous studies of this process [32, 33], we simulate the contributions of  $G_1$  and  $G_2$  to the  $\text{Cs}_2^+$  ions signal obtained after PA in a  $0_g^-(6S_{1/2} + 6P_{3/2})$  level detuned by  $\Delta_L$ , spontaneous emission towards  $v''(a^3\Sigma_u^+)$  bound levels, and ionization with a photon of frequency  $\nu_{\text{ion}}$  of these levels through absorption into levels  $v'$  of the  $(2)^3\Pi_g(6S_{1/2} + 5D_{5/2})$  potential. In this model, the second step of the ionization process is described as a uniform ionization probability of the  $v'$  levels into  $\text{Cs}_2^+$  ions, and will not be considered here. The ionization signal  $S_{\text{ion}}(\Delta_L)$  is expressed as

$$S_{\text{ion}}(\Delta_L) = N_{\text{PA}}(\Delta_L) \sum_{v''} P_{\text{ion}}(v'') \left| \langle \chi_{\bar{v}, \bar{J}}(0_g^-) | \phi_{v''}(a^3\Sigma_u^+) \rangle \right|^2. \quad (7)$$

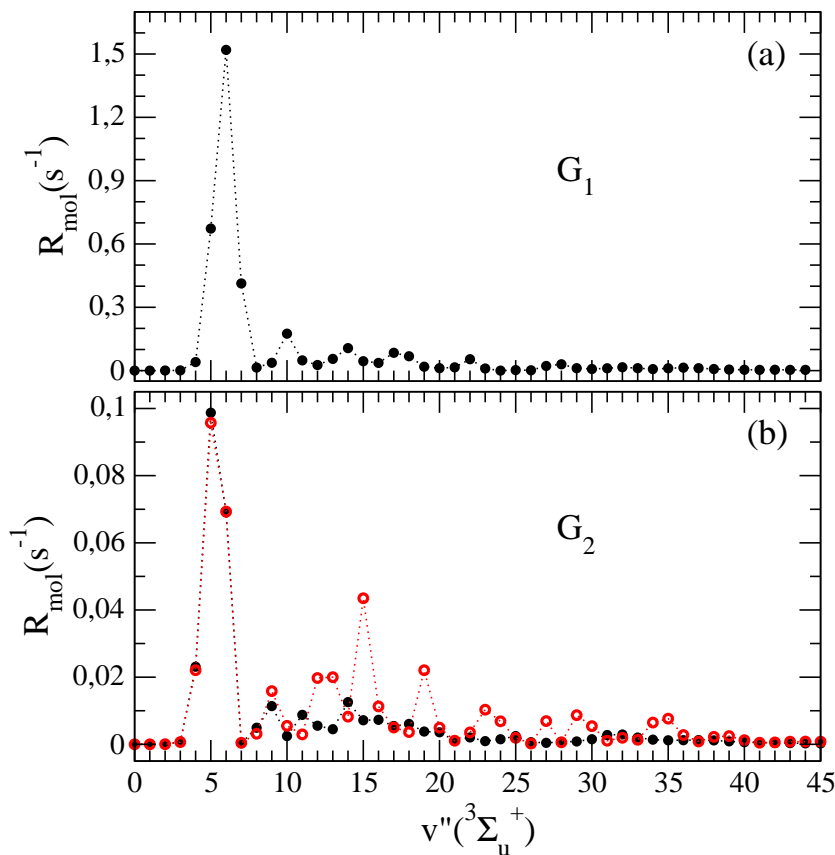


**Figure 5.** Rate of formation of cold molecules in the vibrational levels  $v''(a^3\Sigma_u^+)$ , via photoassociation into (a) the  $G_1$  and (b) the  $G_2$  states. In the latter case, rates for both levels contributing to  $G_2$  are given, i.e., the level at  $-5.87 \text{ cm}^{-1}$  tunneling from the inner wells (black closed circles) and the external level tunneling from the outer well at  $-5.89 \text{ cm}^{-1}$  (red open circles). The calculation is made for  $n_{\text{at}} = 10^{11} \text{ cm}^{-3}$  and an intensity  $I = 100 \text{ W/cm}^2$  for the PA laser.

As in the cold molecules rate calculation, we neglect the  $R$  dependence of the dipole transition moment involved in the spontaneous decay step. In equation (7), the number of molecules  $N_{\text{PA}}(\Delta_L)$  accumulated during the photoassociation step is defined by multiplying the PA rate  $R_{\text{PA}}(\Delta_L)$  with the number of atoms  $n_{\text{PA}}$  in the photoassociation area with the residence time  $t_{\text{PA}}$  of the cold molecules within the trapping region:

$$N_{\text{PA}}(\Delta_L) = R_{\text{PA}}(\Delta_L)n_{\text{PA}}t_{\text{PA}}. \quad (8)$$

In the Cesium PA experiment, typical values for these parameters are  $n_{\text{PA}} = 5 \times 10^7$  and  $t_{\text{PA}} \approx 10 \text{ ms}$ . The excitation probability  $P_{\text{ion}}(v'')$  of the  $v''$  levels into vibrational levels  $v'$  of the  $(2)^3\Pi_g(6S_{1/2} + 5D_{5/2})$  potential is calculated as

$$P_{\text{ion}}(v'') = \sum_{v'} \left| \langle \phi_{v'}(^3\Pi_g) | D | \phi_{v''}(a^3\Sigma_u^+) \rangle \right|^2 f(\nu_{v''v'}), \quad (9)$$

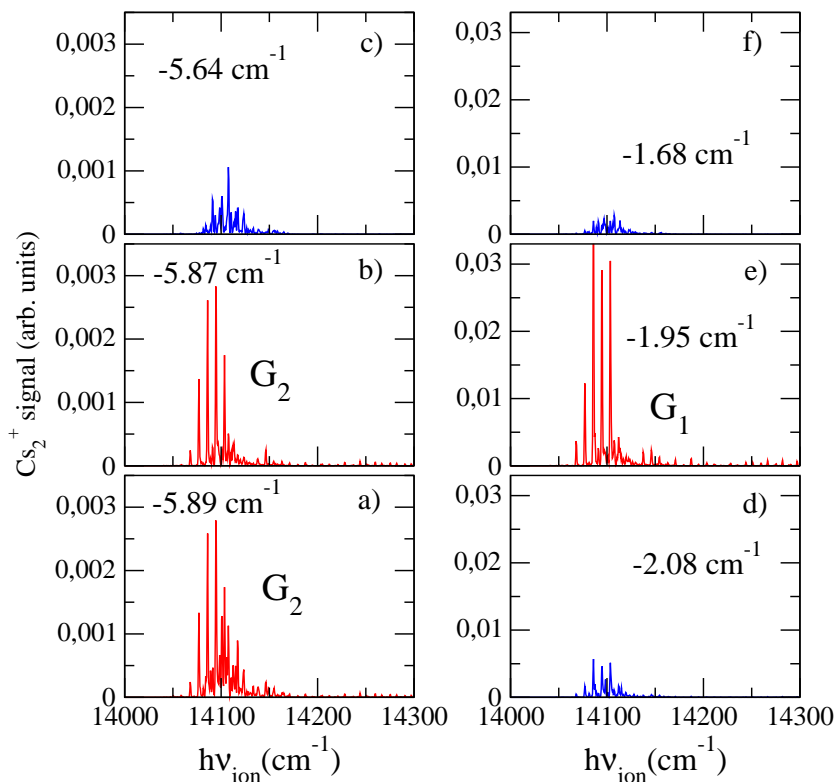


**Figure 6.**  $\text{Cs}_2^+$  ions signal (in arbitrary units) as a function of the frequency of the ionization laser, calculated with equation (7) for detunings  $\Delta_L$  corresponding to  $G_1$  (right column) and  $G_2$  (left column). Signals corresponding to photoassociation in vibrational levels located close to  $G_1$  and  $G_2$  and belonging to the external well of the  $0_g^-(6S_{1/2} + 6P_{3/2})$  potential are also shown. The energy of the  $6S_{1/2} + 5D_{5/2}$  dissociation limit is taken as being  $14597.08 \text{ cm}^{-1}$  above the  $6S_{1/2} + 6S_{1/2}$  origin.

where  $D$  is the  $R$ -dependent dipole moment for the  $a^3\Sigma_u^+ \rightarrow ^3\Pi_g(6s + 5D_{5/2})$  transition calculated in [26], and

$$f(\nu_{v''v'}) = \exp \left[ -\ln(2) \frac{(\nu_{v''v'} - \nu_{\text{ion}})^2}{(\delta\nu)^2} \right] \quad (10)$$

is a parametric function accounting for the resolution of the experiment, estimated at  $\delta\nu \approx 30 \text{ GHz}$  [32], and  $\nu_{v''v'}$  is the transition frequency between  $v''$  and  $v'$  levels.

The ion signals as a function of the ionization frequency  $\nu_{\text{ion}}$  obtained for  $G_1$  and  $G_2$  are displayed in figure 6, together with those corresponding to PA in neighboring vibrational levels  $v_{\text{ext}}$  of the  $0_g^-(6S_{1/2} + 6P_{3/2})$  external well. As expected, large amounts of molecular ions are detected only for specific frequencies corresponding to the resonance condition in the first step. The signals coming from  $G_1$  and  $G_2$  are clearly more intense than those of the surrounding levels, in agreement with the experimental spectrum [20], because of the increased efficiency for forming cold molecules in bound levels of the triplet state. The signal corresponding to  $G_1$ , having a maximum of 0.03 in figure 6e, is five times bigger than the simulated  $G_2$  signal, whose maximum reaches 0.006 if we take the sum of the two contributing levels (figures 6a,b). This ratio

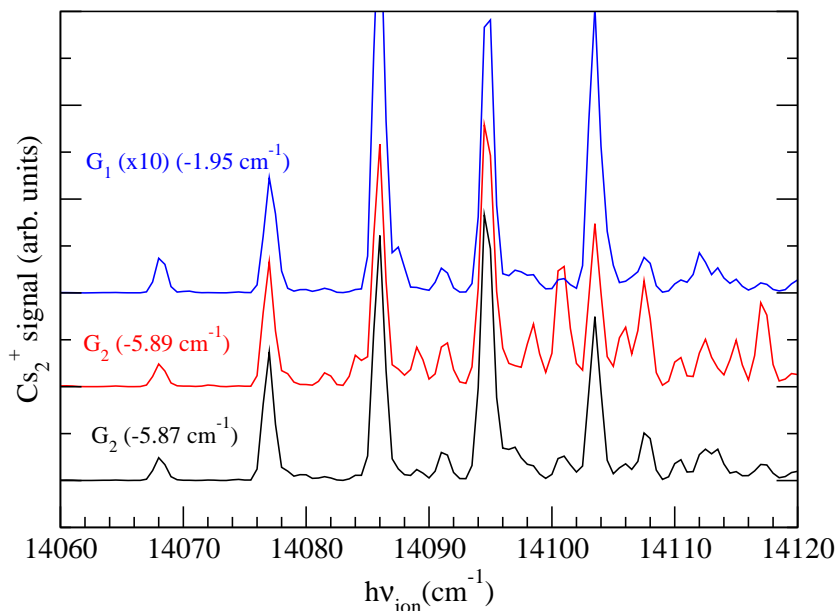


**Figure 7.** Same as figure 6: we superimposed predicted ion signals from panels a, b, and e of this figure, slightly shifted from each other for better visibility. Note that the signal for  $G_1$  is shown at 1/10th of its actual value.

between the intensities of the simulated “giant lines” is larger than in the experimental spectrum where the ratio is only two [25]. This could be due to the fact that the ionization spectra for the tunneling resonances do not match perfectly: the differences in vibrational distributions  $v''(a^3\Sigma_u^+)$  of  $G_1$  and  $G_2$  (see figure 5) make it possible to chose an ionization frequency (e.g.,  $h\nu_{\text{ion}} \approx 14101$  or  $14117 \text{ cm}^{-1}$ ) such that the ratio between the two ion signals is greatly modified, as shown in figure 7.

## 5. Conclusion

As demonstrated through several studies [5, 20, 33], cesium atoms are well-suited for ultracold molecule formation through photoassociation, mainly due to the peculiarity of some of the excited states of the  $\text{Cs}_2$  molecule. Of particular interest is the  $0_g^-(S_{1/2}+P_{3/2})$  state, which is composed of two potential wells separated by a barrier whose height culminates at an energy close to the dissociation asymptote. This allows for tunneling between the two wells, enabling a pair of atoms initially far apart to come close together in a photoassociated molecule.

We have shown here that this tunneling process leads to strongly bound ultracold cesium molecules in the metastable  $a^3\Sigma_u^+(S_{1/2} + S_{1/2})$  ground electronic state. Indeed, it is mostly vibrational levels around  $v'' = 5, 6$  that are populated, in contrast to what can be reached for non-tunneling states of the external  $0_g^-(P_{3/2})$  well ( $v'' > 23$  [22]). The tunneling efficiency is seen to be markedly dependent upon the rotational state  $J$ , in agreement with what was observed experimentally [20].

Finally, we have investigated that the experimental detection scheme, resonant two-

photon ionization, influences the observation of ultracold Cs<sub>2</sub> molecules. Evidence would suggest that the detection process affects the relative intensities seen in the signal, as was the case previously [33]. In other words, the molecules produced are not all ionized with the same efficiency, and it is therefore important to consider this step in the analysis of photoassociation experiments.

## Acknowledgments

This work has been performed in the framework of the Research and Training Network of the European Union “Cold Molecules” (contract number HPRN-CT-2002-00290). O.D. and M.V. acknowledge partial support from the INTERCAN and QUEDDIS networks of the European Science Foundation.

## References

- [1] Anderson M H, Ensher J R, Matthews M R, Wieman C E and Cornell E A 1995 *Science* **269** 198
- [2] Bradley C C, Sackett C A, Tollett J J and Hulet R G 1995 *Phys. Rev. Lett.* **75** 1687
- [3] Davis K B, Mewes M O, Andrews M R, van Druten N J, Durfee D S, Kurn D M and Ketterle W 1995 *Phys. Rev. Lett.* **75** 3969
- [4] DeMarco B and Jin D S 1999 *Science* **285** 1703
- [5] Fioretti A, Comparat D, Crubellier A, Dulieu O, Masnou-Seeuws F and Pillet P 1998 *Phys. Rev. Lett.* **80** 4402
- [6] Bethlem H L, Berden G, Cromptoets F M H, Jongma R T, van Roij A J A and Meijer G 2000 *Nature* **406** 491
- [7] Weinstein J D, deCarvalho R, Friedrich T G B and Doyle J M 1998 *Nature* **395** 148
- [8] Rangwala S A, Junglen T, Rieger T, Pinkse P W H and Rempe G 2003 *Phys. Rev. A* **64** 043406
- [9] Elioff M S, Valentini J J and Chandler D W 2003 *Science* **302** 1940
- [10] Gupta M and Herschbach D 1999 *J. Phys. Chem. A* **103** 10670
- [11] Jochim S, Bartenstein M, Altmeyer A, Hendl G, Chin C, Hecker Denschlag J and Grimm R 2003 *Phys. Rev. Lett.* **91** 240402
- [12] Zwierlein M W, Stan C A, Schunck C H, Raupach S M F, Gupta S, Hadzibabic Z and Ketterle W 2003 *Phys. Rev. Lett.* **91** 250401
- [13] Staanum P, Kraft S D, Lange J, Wester R, and Weidemüller M 2006 *Phys. Rev. Lett.* **96** 023201
- [14] Zahzam N, Vogt T, Mudrich M, Comparat D, and Pillet P 2006 *Phys. Rev. Lett.* **96** 023202
- [15] Thorsheim H R, Weiner J and Julienne P S 1987 *Phys. Rev. Lett.* **58** 2420
- [16] Tsai C C, Freeland R S, Vogels J M, Boesten H M J M, Gardner J R, Heinzen D J and Verhaar B J 1997 *Phys. Rev. Lett.* **79** 1245
- [17] Laburthe Tolra B, Drag C and Pillet P 2001 *Phys. Rev. A* **64** 061401(R)
- [18] Nikolov A N, Ensher J R, Eyler E E, Wang H, Stwalley W C and Gould P L 2000 *Phys. Rev. Lett.* **84** 246
- [19] Sage J M, Sainis S, Bergeman T and DeMille D 2005 *Phys. Rev. Lett.* **94** 203001
- [20] Vatasescu M, Dulieu O, Amiot C, Comparat D, Drag C, Kokoouline V, Masnou-Seeuws F and Pillet P 2000 *Phys. Rev. A* **61** 044701
- [21] Vatasescu M and Masnou-Seeuws F 2002 *Eur. Phys. J. D* **21** 191
- [22] Drag C, Laburthe Tolra B, Dulieu O, Comparat D, Vatasescu M, Boussem S, Guibal S, Crubellier A and Pillet P 2000 *IEEE J. Quant. Electron.* **36** 1378
- [23] Comparat D 1999 Ph.D. Thesis Université Paris XI
- [24] Gutterres R, Amiot C, Fioretti A, Gabbanini C, Mazzoni M and Dulieu O 2002 *Phys. Rev. A* **66** 024502

- [25] Fioretti A, Comparat D, Drag C, Amiot C, Dulieu O, Masnou-Seeuws F and Pillet P 1999 *Eur. Phys. J. D* **5** 389
- [26] Spies N 1989 Ph.D. Thesis Universität Kaiserslautern
- [27] Kokoouline V, Dulieu O, Kosloff R and Masnou-Seeuws F 1999 *J. Chem. Phys.* **110** 9865
- [28] Foucrault M, Millié P and Daudey J-P 1992 *J. Chem. Phys.* **96** 1257
- [29] Marinescu M 1994 *Phys. Rev. A* **50** 3177
- [30] Kerman A J, Chin C, Vuletić V, Chu S, Leo P J, Williams C J and Julienne P S 2001 *C. R. Acad. Sci. Paris* **2** 633
- [31] Pillet P, Crubellier A, Bleton A, Dulieu O, Nosbaum P, Mourachko I and Masnou-Seeuws F 1997 *J. Phys. B* **30** 2801
- [32] Dion C M, Dulieu O, Comparat D, de Souza Melo W, Vanhaecke N, Pillet P, Beuc R, Milošević S and Pichler G 2002 *Eur. Phys. J. D* **18** 365
- [33] Dion C, Drag C, Dulieu O, Laburthe Tolra B, Masnou-Seeuws F and Pillet P 2001 *Phys. Rev. Lett.* **86** 2253